

Green Chemistry

Accepted Manuscript



This article can be cited before page numbers have been issued, to do this please use: S. Zhou, G. Chen, X. Feng, M. Wang, T. Song, D. Liu, F. Lu and H. Qi, *Green Chem.*, 2018, DOI: 10.1039/C8GC01413B.



This is an Accepted Manuscript, which has been through the Royal Society of Chemistry peer review process and has been accepted for publication.

Accepted Manuscripts are published online shortly after acceptance, before technical editing, formatting and proof reading. Using this free service, authors can make their results available to the community, in citable form, before we publish the edited article. We will replace this Accepted Manuscript with the edited and formatted Advance Article as soon as it is available.

You can find more information about Accepted Manuscripts in the [author guidelines](#).

Please note that technical editing may introduce minor changes to the text and/or graphics, which may alter content. The journal's standard [Terms & Conditions](#) and the ethical guidelines, outlined in our [author and reviewer resource centre](#), still apply. In no event shall the Royal Society of Chemistry be held responsible for any errors or omissions in this Accepted Manuscript or any consequences arising from the use of any information it contains.



Green Chemistry

ARTICLE

In situ MnO_x/N-doped carbon aerogels from cellulose as monolithic and highly efficient catalysts for upgrading of bioderived aldehydes

Received 00th January 20xx,
Accepted 00th January 20xx

DOI: 10.1039/x0xx00000x

www.rsc.org/

Shenghui Zhou^a, Guixian Chen^a, Xiao Feng^a, Ming Wang^a, Tao Song^a, Detao Liu^a, Fachuang Lu^{a,b} and Haisong Qi^{*a,b}

Herein, we report a sustainable route to *in-situ* synthesize a monolithic MnO_x/N-doped carbon aerogel catalyst (Mn-NCA) by pyrolyzing MnO(OH)₂-cellulose aerogel precursor based on an alkali-urea aqueous system. The as-obtained Mn-NCA furnish highly efficient catalytic activity for transfer hydrogenation of a broad scope of biomass-derived aldehydes, yielding 90–100% conversion and 64–100% selectivity to corresponding alcohols under mild conditions in an oven without agitation. Combination of controlled experiments and detailed characterizations indicates that the superior performance of Mn-NCA is attributed to the monolithic three-dimensional (3D) hierarchical porous architecture and the synergistic effects between homogeneously dispersed MnO_x nanoparticles (NPs) and urea-derived basic sites. The monolithic feature of Mn-NCA exhibits more excellent dispersibility and separability compared to conventional centrifugation and filtration techniques in powdery catalytic system. Moreover, a possible reaction mechanism is proposed. Our work provides a new approach for developing highly efficient monolithic catalysts from renewable biopolymers for biomass valorization.

Introduction

The excessive exploitation and utilization of depleted fossil resources have been causing serious energy crisis, increasing emission of greenhouse gases and severe environmental pollution.¹ Upgrading of optimal inexhaustible biomass-derived platform chemicals into bio-fuels and value-added chemicals has received significant attention, as a means to link raw biomass to the sustainable chemical industry and alleviate heavily energy dependence on non-renewable fossil resources.² For instance, furfural (FF) and 5-hydroxymethylfurfural (5-HMF), which can be obtained by the acid-catalyzed dehydration of hemicellulose and cellulose-derived carbohydrates, respectively, are identified as appealing versatile feedstocks to manufacture high-value products through various reactions.^{3–5} Especially, selective transformation of FF to furfuryl alcohol (FA) and 5-HMF to 2,5-bis-(hydroxymethyl)-furan (BHMF) exhibits great practical application value in biorefinery.^{6,7} Because, FA and BHMF can be used as important precursors for production of synthetic

fibers, crown ethers, resins, drugs, adhesives or as intermediates for further transformation into liquid biofuel.^{8,9}

There were many efforts reported about the catalytic transformations of biomass platform compounds via hydrogenation or hydrodeoxygenation using hydrogen gas as the H-donor catalyzed by transition metals.^{10,11} However, the use of flammable and explosive H₂ with high pressure and temperature, uncontrollable and unsatisfactory selectivity toward targeted products owing to overhydrogenation and C–C cleavage impels us to explore alternative process.^{12,13} More recently, catalytic transfer hydrogenation (CTH) using organic hydrogen-donors, such as alcohols and formic acid, to replace dangerous gaseous hydrogen has emerged as an attractive strategy for the reductive upgrading of biomass-derived aldehydes.^{8,14} Particularly, the utilization of alcohols as both H-donor and solvent offers significant advantages such as cheap, abundance, easy storage and easy to remove when compared with corrosive formic acid.^{15,16} In recent years, several homogeneous Mn catalysts (e.g. manganese pincer complexes) have been employed in CTH reaction of aldehydes, but it is difficult to recycle and reuse the homogeneous catalysts.^{17,18} Various powdery catalysts based on Fe,¹⁹ Co,⁸ Ni,²⁰ Cu,^{21,22} Al,²³ Zr,²⁴ Hf,²⁵ Pd,²⁶ Ru²⁷ and others have been applied for CTH of bioderived aldehydes with alcohols as hydrogen donor. However, the recovery of catalysts via filtration or centrifugation techniques was time-consuming and less energy-saving. Meanwhile, loss of solid catalysts was inevitable in the separation process. These issues limited its application.^{28,29} To overcome these disadvantages, lots of

^a State Key Laboratory of Pulp and Paper Engineering, South China University of Technology, Guangzhou 510640, China. E-mail: qhs@scut.edu.cn.

^b Guangdong Engineering Research Center for Green Fine Chemicals, Guangzhou 510640, China.

† Footnotes relating to the title and/or authors should appear here.

Electronic Supplementary Information (ESI) available: [details of any supplementary information available should be included here]. See DOI: 10.1039/x0xx00000x

magnetic nanocatalysts were developed and employed in the fields of biorefinery.^{30,31} However, tedious functionalization procedure of magnetic nanoparticles was essential and an external magnetic field was still necessary for the recovery of catalysts.²⁸ Therefore, it is still meaningful and imperative to develop easily recoverable and recyclable, more efficient and low-cost heterogeneous catalysts to increase the feasibility of biomass transformation on an industrial scale.

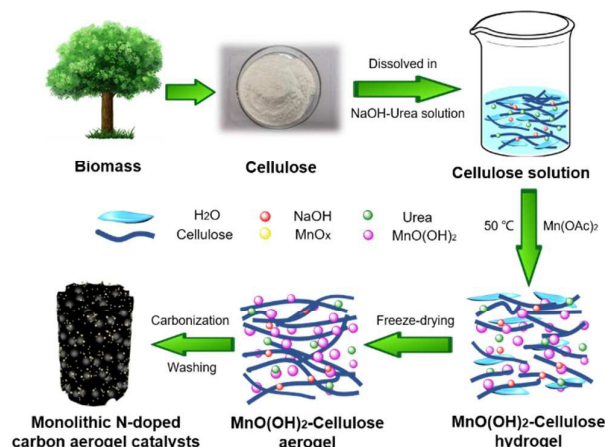
Cellulose which can be obtained from woods and agricultural waste, is environmentally benign, biodegradable and the most abundant part of lignocellulosic biomass. Due to the strong intra- and intermolecular hydrogen bonds interactions, cellulose is insoluble in water and conventional solvents, making it difficult for material manufacture.³² In recent years, a variety of solvents including N,N-dimethylacetamide (DMAC)/LiCl,³³ dimethylsulfoxide (DMSO)/LiCl,³⁴ ionic liquid,³⁵ N-methylmorpholine-N-oxide (NMMO)³⁶ and NaOH-urea aqueous solution³⁷ have been developed for dissolving cellulose. Among these solvents, the alkali-urea solution is the most powerful aqueous solvent and is economic and environment friendly based on our previous work.^{32,38,39}

Herein, we report a novel and sustainable strategy to *in-situ* synthesize MnO_x NPs supported N-doped carbon aerogel (Mn-NCA) by dissolving cellulose and manganese acetate in NaOH-urea aqueous system, followed by a carbonization process. The dissolving process of cellulose is crucial for the formation highly active Mn-NCA catalysts in many aspects, including (1) Transformation of powdery cellulose to carbon aerogel through dissolving, gelling and carbonization process endowed the catalysts with monolithic property; (2) NaOH as activating agent promoted the formation of 3D hierarchically porous structure with large specific surface area; Basic sites derived from urea provided excellent synergistic catalytic effects with MnO_x NPs; (3) MnO(OH)₂, NaOH and urea could be uniformly dispersed in cellulose solution, subsequently, resulting in the homogeneous doping of nitrogen and highly dispersion of MnO_x NPs. Owing to these unique characters, the Mn-NCA exhibited remarkable catalytic activity for CTH of bioderived aldehydes to alcohols in an oven without agitation. In detail, the influence of chemical composition and particularly the pyrolysis temperature of MnO(OH)₂-cellulose aerogel precursor on catalytic performance of Mn-NCA were comprehensively investigated. Additionally, the reaction kinetics and plausible mechanism were also studied.

Results and discussion

Preparation and characterization of monolithic carbon aerogel catalysts

The designed procedure for the *in-situ* fabrication of Mn-NCA is illustrated in **Scheme 1**. Herein, abundant cellulose and Mn(CH₃COO)₂·4H₂O were used as carbon source and Mn source. NaOH-urea aqueous solution was selected as the dispersion medium and the solution of cellulose. Firstly, 4g powdery cellulose



Scheme 1 Schematic illustration of synthesis of Mn-NCA catalyst.

fibers were rapidly dissolved into 100g pre-cooled NaOH-urea aqueous solution (7wt.%,12wt.%) to obtain a transparent and sticky cellulose solution. Subsequently, manganese acetate solution (7.3mmol in 12g water) was added and the sol was then heated for further gelation. During these characteristic dissolving and gelling processes, strong intra and inter molecular hydrogen bonds in compact cellulose fibers with high crystallinity were broken and restructured. The cellulose chains could be aggregated into interconnected nanofibrils with uniformly dispersion of MnO(OH)₂, NaOH and urea. Afterwards, the obtained hydrogel was freeze-dried followed by carbonization at different temperatures (600, 700, 800 °C for 2 h). During this pyrolysis process, nitrogen species derived from urea in cellulose solution were reserved partially and doped into the carbon skeleton. Carbon aerogel was activated through the reaction between NaOH and carbon. MnO(OH)₂ were decomposed into MnO_x NPs (MnO(OH)₂ → MnO_x + H₂O). Finally, monolithic Mn-NCA catalysts was obtained by washing with deionized water to remove residual chemicals.

The structure, composition, morphology and physical-chemical properties about Mn-NCA-T (T stands for the carbonization temperature) materials were characterized by several techniques. N₂ adsorption/desorption isotherms showed that all the samples display a type-I plus type-IV curve

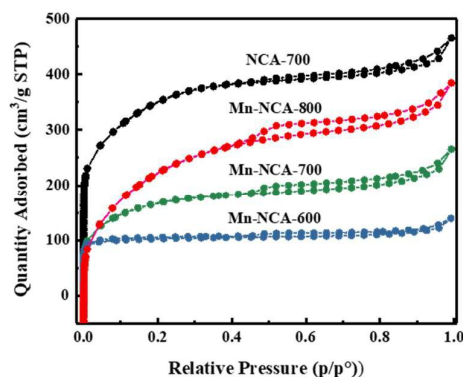


Fig. 1 Nitrogen adsorption–desorption isotherms of Mn-NCA-T.

and an obvious H3-type hysteresis loop in $0.4 < P/P_0 < 1.0$ (Fig. 1).⁴⁰ These results indicated the presence of micro/mesopore structures, which was also confirmed by their corresponding pore-size distribution curves (Fig. S1). The texture properties in Table S1 showed that Mn-NCA-700 had medium surface area ($676.95 \text{ m}^2/\text{g}$), pore volume ($0.41 \text{ cm}^3/\text{g}$) and maximum average pore diameter (4.89 nm) in Mn-NCA-T. The chemical composition of all the catalysts were measured by ICP-OES and elemental analyzer. As shown in Table S2, the metal and N contents of all catalysts were varied in the range of 13–30 wt.% and 0.5–7wt.%, respectively. Therefore, the pyrolysis temperature significantly influenced the physical structure and chemical composition of catalysts. The large specific surface area and pore size in the Mn-NCA-700 would be helpful to expose more active sites and improve the mass transfer of reaction molecules.

The X-ray diffraction (XRD) patterns of the as-obtained NCA-700 and Mn-NCA-T were presented in Fig. 2. A broad diffraction peak observed at 24° in NCA-700 can be attributed to the (002) planes of amorphous graphitic carbon, indicating partial crystallisation of amorphous carbon to graphite.⁴¹ It can be observed that the Mn-NCA-700 and Mn-NCA-800 displayed the similar diffraction peaks. The characteristic peaks at 18.0° , 28.9° , 32.3° , 36.1° , 44.4° , 50.7° , 60.6° , and 64.7° belong to the (101), (200), (103), (202), (220), (105), (215), and (400) lattice planes of the Mn_3O_4 (JCPDS card No. 24-0734). The peaks at 34.9° , 40.6° , 58.7° , 70.2° , and 73.8° belong to the (111), (200), (220), (311), and (222) lattice planes of the MnO (JCPDS card No. 78-0424). At the same time, it is quite interesting to note that Mn_3O_4 phase cannot be indexed in the sample of Mn-NCA-600. The possible reason is that the most of formed Mn_3O_4 was reduced into MnO in the presence of sufficient carbon due to few carbons were consumed by activating agent NaOH under relatively low temperatures.

The morphology and microstructure of the NCA-700 and Mn-NCA-700 were then examined by SEM and TEM. It can be found in SEM image (Fig. 3a and 3b) that, both NCA-700 and Mn-NCA-700 had a typical three-dimensional (3D) hierarchical porous frameworks with plentiful continuous interconnected

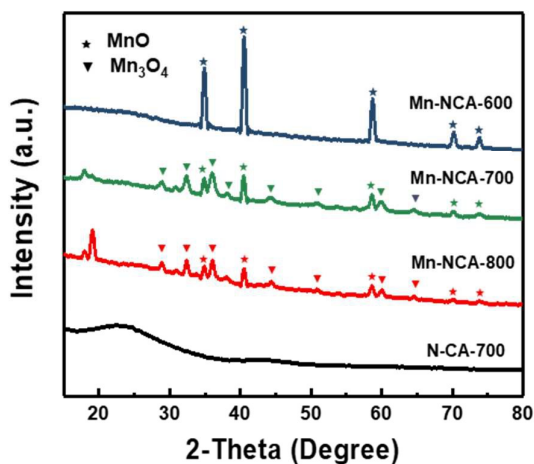


Fig. 2 XRD patterns of NCA-700 and Mn-NCA-T.

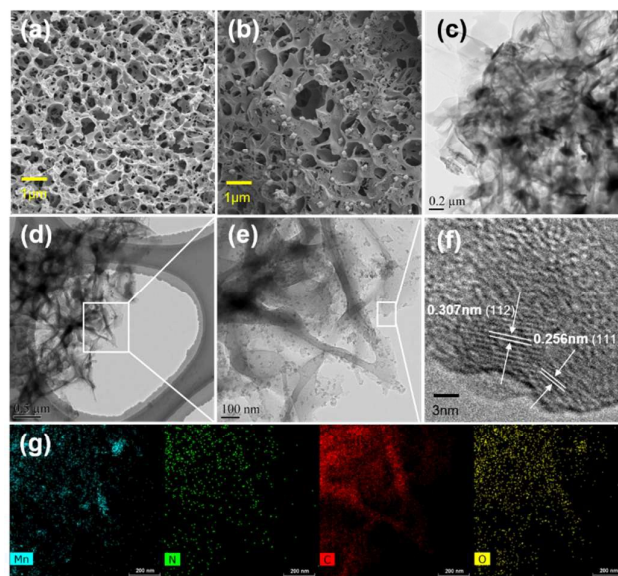


Fig. 3 SEM images of NCA (a) and Mn-NCA-700 (b). TEM images of Mn-NCA-700 (c-f) and corresponding element mapping images (g) of (e).

macropores. As clearly observed in Fig. 3b that, furthermore, MnO_x particles with sizes of 100–200 nm were uniformly anchored onto the channel of 3D carbon aerogel in Mn-NCA-700 which was consistent with particles observed in low magnification TEM images (Fig. 3c). These relatively large particles were unfavourable for the dispersion of active sites and the research on inhibiting the agglomeration of nanoparticles are now in progress. High magnification TEM image (Fig. 3e) showed that a great quantity of ultra-small MnO_x NPs with an average particle size of about 20 nm were highly dispersed on the carbon aerogel support. In accordant with the XRD result, the lattice fringes in Fig. 3f were clearly observed with the interplanar spacings of 0.307 nm and 0.256 nm, corresponding to the (211) planes of Mn_3O_4 crystals and the (111) planes of the MnO phases, respectively. The EDS mapping images from representative high-angle annular dark-field scanning TEM (HAADF-STEM) were shown in Fig. 3g, which confirmed that Mn, N, C and O elements were homogeneously distributed in Mn-NCA-700.

For comparison, the SEM and TEM images of Mn-NCA-600 and Mn-NCA-800 were presented in Fig. S2 and S3, respectively. Mn-NCA-600 showed monolithic block structure with very few crosslinked macropores and dispersed manganese oxide particles in the surface due to incomplete activation of carbon aerogel under low pyrolysis temperature. When the pyrolysis temperature rose to 800°C , both of 3D porous frameworks with a large number of macropores and some very large aggregated particles (about $1\mu\text{m}$) could be observed. In our cases, the temperature of 700°C was relatively favourable for the formation of porous carbon aerogel structure with highly dispersed MnO_x NPs.

The Raman spectra in Fig. 4 showed that all samples exhibited two wide peaks at 1596 and 1354 cm^{-1}

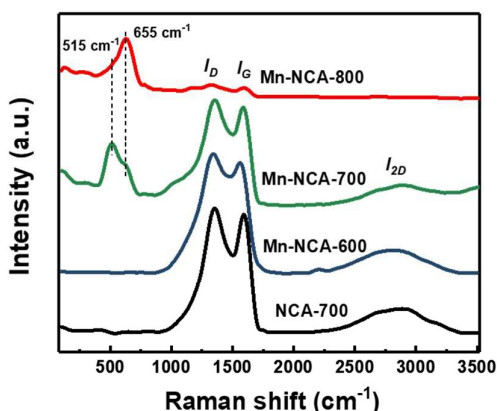


Fig. 4 Raman spectra of NCA-700 and Mn-NCA-T.

corresponding to G and D bands of graphitization carbon, respectively.⁴² In addition, a broader 2D peak appeared at around 2750 cm^{-1} , which was consistent with that of the nitrogen-doped carbon material reported. The 2D band is a prominent feature of higher graphitic degree.⁴³ It can be found that Mn-NCA-700 had the lowest I_D/I_G (1.006) and the highest I_{2D}/I_G (0.6690) in Mn-NCA-T (Table S1), indicating the lower defects and higher graphitic degree of Mn-NCA-700. Additionally, the scattering peak located at 655 cm^{-1} in Mn-NCA-700 and Mn-NCA-800 could be attributed to characteristic peaks of high crystallized MnO_x NPs. This peak shifted to 515 cm^{-1} and the peak shape became broader in Mn-NCA-700, indicating a higher dispersion of the MnO_x NPs.⁴⁴ Fig. S4 presented the FT-IR spectra of the NCA and Mn-NCA-T samples. For all the samples, the peaks around 1200 cm^{-1} , 1600 cm^{-1} were ascribed to the stretches of the C-OH stretching vibration, and the aromatic C=C stretching vibration, respectively.⁴⁵ These two peaks became stronger under low pyrolysis temperature, indicating the existence of large numbers of residual hydroxyl groups and aromatic C=C due to incomplete carbonization.⁴⁶ In addition, two new absorption bands in Mn-NCA-T were observed at 624 cm^{-1} and 518 cm^{-1} , which were associated with the coupling of Mn-O stretching modes of tetrahedral and octahedral sites.⁴⁷ These results further confirm the existence of manganese oxide in Mn-NCA-T, well corresponding to the results of other characterizations.

X-ray photoelectron spectroscopy (XPS) tests were further carried out to gain the electronic states of all elements and estimate the proportion of Mn^{2+} and Mn^{3+} in the Mn-NCA-T (Fig. 5). The survey spectra confirmed the existence of the Mn, N, C and O elements in Mn-NCA-T (Fig. S5a). Fig. 5a shows the high-resolution Mn $2p_{3/2}$ peak of Mn-NCA-T, and this peak could be deconvoluted into two peaks located at 640.9 and 642.4 eV, which were assignable to Mn^{2+} and Mn^{3+} species, respectively.⁴⁸ XPS results revealed that Mn-NCA-700 exhibited maximum proportion (70%) of Mn^{3+} among Mn-NCA-T. It may be due to that high-valence Mn^{3+} was mostly reduced into Mn^{2+} by sufficient carbon under relatively low temperatures ($\text{Mn}^{3+} + \text{C} \rightarrow \text{Mn}^{2+} + \text{CO}_2$). However, high temperature also enhanced the redox reaction between MnO_x NPs and carbon.

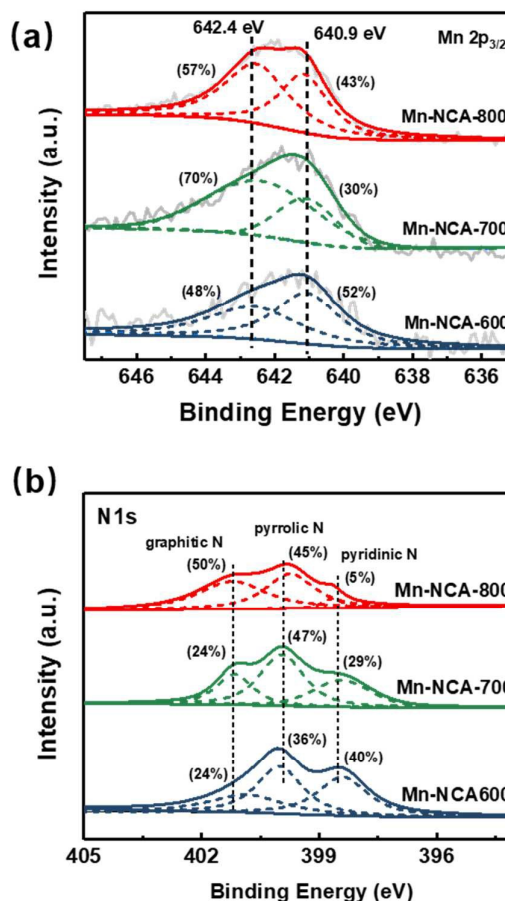


Fig. 5 XPS spectrum of Mn $2p_{3/2}$ peaks (a) and N 1s peak (b) of Mn-NCA-T.

Therefore, 700 °C was more suitable for the formation of high-valence MnO_x in this study. The N 1s spectrum of Mn-NCA-T catalyst in Fig. 5b could be deconvoluted into three different types of nitrogen species, corresponding to pyridinic-N (398.5 eV), pyrrolic-N (400.0 eV) and graphitic-N (401.25 eV), respectively.⁴⁹ Noticeably, the percentage of pyridinic-N decreased as the pyrolysis temperature increased and the graphitic-N became the dominant phase in Mn-NCA-800, indicating the transformation of pyridinic-N to graphitic-N under high temperatures. In addition, the N 1s spectrums of recycled and grinded Mn-NCA-700 catalyst were almost the same as that of fresh catalyst (Fig. S5d), indicating that high stability of nitrogen species. As reported, the doped-nitrogen can reduce the energy barrier for reactants adsorption and accelerate the electron transfer, which led to a significant enhancement of the catalytic activity of the carbon surface.⁵⁰ In this work, we speculated that doped nitrogen in the Mn-NCA-T catalyst should act as basic sites, which could be beneficial to enhance the generation and transfer of proton from 2-propanol. The C 1s spectrum presented in Fig. S5b was fitted into four parts arising from C-C/C=C (284.0 eV), C-O (285.4 eV), C-N (285.8 eV), and C=O (289.2 eV) groups,

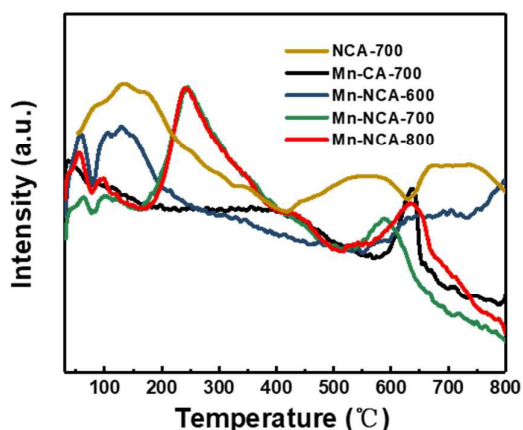


Fig. 6 CO₂-TPD profiles for Mn-CA-700 and Mn-NCA-T.

respectively.⁵¹ As for the O 1s region in Fig. S5c, three main peaks located at around 530.2 eV, 532.3 and 533.1 eV in the deconvolution spectrum, corresponding to manganese oxide (Mn–O), hydroxyl bonding to Mn (Mn–OH) and C–OH bonds, respectively.⁵²

Then we further performed CO₂-TPD to analyze the surface basicity of samples. As shown in Fig. 6, three obvious desorption peaks centered at around 70 °C, 120 °C and 260 °C in NCA-700, Mn-NCA-700 and Mn-NCA-800. These peaks were correspondingly attributed to weak basic sites, medium basic sites and medium-strength basic sites. As for Mn-CA-600, only weak basic sites and medium basic sites were formed. It was worth noting that Mn-CA-700 exhibited no peaks compared with other samples, implying the inexistence of basic sites. These results demonstrated that urea in cellulose solution played a crucial role in the formation of basic sites in Mn-NCA-T and the pyrolysis temperature also influenced the strength of the basic site.

Catalytic performance evaluation of the various catalysts

Subsequently, the transfer hydrogenation of FF with 2-propanol was chosen as a model reaction to assess the activity of various catalysts and the results were shown in Table 1. The blank run showed that very small amount of FF (4%) was transformed and the selectivity of FA was zero in the absence of any catalyst (Table 1, Entry 1). The GC–MS analysis of the product showed that the aldol condensation product (4-(2-furyl)-3-buten-2-one and isopropyl 2-furoate) of FF with acetone were the main by-products (Fig. S6). Thus, the CTH of FF was unrealistic without catalysts. Gratifyingly, the catalytic reaction could efficiently proceed when Mn-NCA-700 was added and 98% conversion of FF with 85% FA selectivity was obtained with high turnover frequency (TOF) of 2.58 h⁻¹. (Table 1, Entry 7). To gain insight into the effects of each component in Mn-NCA-700, a series of different catalysts were tested based on CTH of FF. The MnO_x was examined and gave a slightly improved FF conversion (10%) with 82% selectivity to FA and low TOF of 0.26 h⁻¹ (Table 1, Entry 2). In addition, the replacement metal center Mn with Co, Fe, Cu and Ni in

Table 1 Comparison on catalytic performance of different catalysts for FF transfer hydrogenation to FA^a

Entry	Catalysts	Conv. (%)	Sel. (%)		TOF (h ⁻¹) ^c
			FA	Others ^b	
1	Blank	4	0	100	-
2 ^d	MnO _x	10	82	18	0.26
3	CA-700	4	17	83	-
4	NCA-700	16	60	34	-
5	Mn-CA-700	35	68	32	0.92
6	Mn-NCA-600	32	87	13	0.84
7	Mn-NCA-700	98	85	15	2.58
8	Mn-NCA-800	52	71	29	1.37
9 ^e	Mn-NCA-700	60	82	18	1.58
10	Co-NCA-700	89	84	16	2.35
11	Fe-NCA-700	9	64	36	0.24
12	Cu-NCA-700	14	55	45	0.37
13	Ni-NCA-700	35	81	19	0.92

^a Reaction conditions: 0.5mmol FF in 5ml 2-propanol, 160 °C, 1h, catalyst (40 mol% Mn).

^b Others include 4-(2-furyl)-3-buten-2-one and isopropyl 2-furoate (the aldol condensation product of FF with acetone).

^c TOF is defined as mol(converted FF)/[mol(total metal added) × h(time)].

^d MnO_x were prepared by calcination of Mn(CH₃COO)₂·4H₂O at 500 °C in air for 6 h, the reaction autoclave was stirred at 160 °C in oil bath.

^e The monolithic carbon aerogel catalyst was grinded into powder.

Mn-NCA-700 all resulted in inferior catalytic activity for CTH of FF to FA. It indicated the nature of the metallic oxide was crucial for the catalytic performance and MnO_x NPs may be the active sites in CTH (Table 1, Entry 10–13). Moreover, compared to the catalysts without nitrogen doping (CA-700 and Mn-CA-700, Table 1, Entry 3, 5), the N-doped carbon aerogel catalysts (NCA-700 and Mn-NCA-700, Table 1, Entry 4, 7) acquired remarkably improvement in FF conversion and FA selectivity, which suggested that nitrogen species played an important role in enhancing the conversion of FF. The N sites derived from urea in cellulose solution could be reserved partially after pyrolysis, which potentially endowed the catalysts with abundant Lewis basic sites. We speculated that these basic sites could facilitate the generation of proton and deliver the free proton to the activated aldehyde molecules, and thus promote the reaction. In brief, the presence of a synergistic promoting interaction between MnO_x NPs and N-doped carbon aerogel was of vital importance in affecting the catalytic performance of Mn-NCA-700 in transfer hydrogenation of FF.

Interestingly, the results also indicated that the pyrolysis temperature also significantly affected the activity of the Mn-NCA-T. Among these samples, Mn-NCA-700 afforded the highest catalytic activity and TOF value (Table 1, Entry 8). There were mainly two reasons accounting for the better catalytic performance of Mn-NCA-700 than others combining with characterization of catalysts: (1) 3D hierarchical porous structure with large specific surface area and higher mesoporous and macroporous proportion in Mn-NCA-700 were beneficial for exposure of active sites, diffusion and transportation of reaction molecules, thus could significantly improve the reaction rate; (2) The pyrolysis temperature significantly affected the degree of dispersion of MnO_x NPs and the electronic states of manganese. The most of Mn₃O₄ was converted into MnO in the presence of sufficient carbon due to few carbons were consumed by activating agent NaOH under relatively low temperatures (confirmed by XRD patterns and XPS spectrum). While pyrolysed at 800 °C, the isolated active sites in Mn-NCA tended to aggregate (confirmed by SEM and TEM images). It was worth noting that, the conversion of FF greatly decreased when the Mn-NCA-700 catalyst used was grinded into powder (Table 1, Entry 9). Compared with the reported other reported powdery catalysts (Table S3), the monolithic carbon aerogel catalyst could efficiently catalyze the reaction in an oven without agitation with comparative conversion and selectivity under mild conditions. Moreover, the monolithic catalytic system was energy-efficient and timesaving and showed great advantage in the operation of reaction and separation of catalyst.

Effects of reaction temperature and time and reaction kinetics study

The influence of reaction time and temperature on synthesis of FA from FF catalyzed by Mn-NCA-700 was also investigated. As shown in Fig. 7a and b, the conversion of FF was remarkably elevated with an increase in reaction temperature from 403 to 473 K. For example, only 8% of FF conversion with 65% of FA selectivity was obtained if the reaction was conducted at 403 K for 10 min, whereas a much higher 57% conversion of FF with 87% of FA selectivity could be achieved if the reaction temperature was increased to 473 K in a reaction time of 10 min. Additionally, the reaction time also had a large influence on the reaction. It could reach nearly full conversion of FF (99%) and 85% of FA selectivity by prolonging the reaction time to 1 h at 433 K. As shown in Fig. 7b, meanwhile, aldol condensation products as the side product gradually decreased with the increase of the reaction temperature. These results indicate that higher temperature promoted the equilibrium shift from the aldol condensation product to FA. In addition, when the temperature was increased to 473 K, the selectivity of FA increased firstly and then gradually declined due to overhydrogenation of FA to 2-methylfuran and tetrahydrofuran with the increase of reaction time.

To further determine the apparent activation energy (E_a) of FF transfer hydrogenation, its kinetics was investigated over

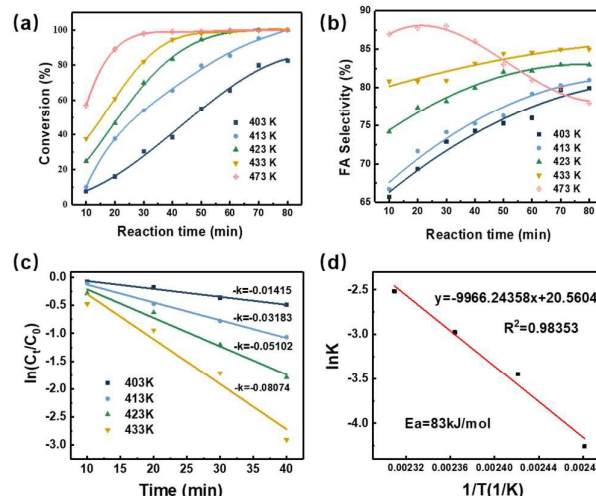


Fig. 7 Effects of reaction temperature and time on conversion of FF (a) and selectivity of FA (b) over the Mn-NCA-700. First-order kinetic fit (c) for the CTH of FF to FA at different temperatures and corresponding Arrhenius plots (d) for Mn-NCA-700. Reaction conditions: 0.5mmol FF in 5ml 2-propanol, 55mg Mn-NCA-700 catalyst.

the temperature range 403–433 K. The rate formula of FF transfer hydrogenation could be expressed by the following Eq. (1) since the catalyst amount was a constant and 2-propanol with an extremely higher concentration compared to FF. Hypothesizing that the reaction was a first-order reaction ($\gamma = 1$), c_0 was the initial concentration of FF and c_t was the concentration of FF after a reaction time of t , and thus Eq. (1) could be expressed as Eqs. (2) or (3). Experiment results demonstrated the $\ln(c_0/c_t)$ had a linear relationship with t . As compiled in Fig. 7c, reaction rate constants (k) were determined at each temperature from the corresponding slope of the plots. According to Arrhenius equation and its variable formula (4), the apparent activation energy E_a was calculated to be 83 kJ/mol from the corresponding Arrhenius plot presented in Fig. 7d. The low activation energy of the Mn-NCA-700 should be related to the synergistic effects between MnO_x NPs and N-doped carbon aerogel.

$$r = -dc_t/dt = k \cdot [\text{FF}]^\gamma, k = k_0 \cdot [\text{Cat}]^\alpha \cdot [2\text{-propanol}]^\beta \quad (1)$$

$$r = -dc_t/dt = k \cdot [\text{FF}] \quad (2)$$

$$\ln(c_0/c_t) = -k \cdot t \quad (3)$$

$$\ln k = \ln A - E_a/RT \quad (4)$$

Effects of the catalyst dosage, heterogeneity and recyclability of Mn-NCA catalyst

The effect of catalyst dosage on CTH of FF into FA was also examined (Fig. S7). The selectivity toward FA increased from 79 to 84% with the elevated catalyst dosage from 30–55 mg. Further increasing the amount of catalyst to 125mg led to obvious decrease in the selectivity to FA (80%) with complete transformation of FF. Moreover, the heterogeneous nature of Mn-NCA-700 in the catalytic process was assessed by removing

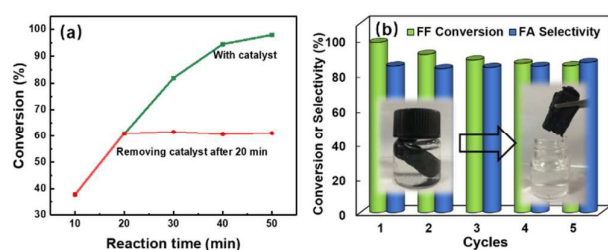


Fig. 8 Heterogeneity (a) and reusability (b) of the Mn-NCA-700 catalyst.

the catalyst from the mixture after 20 min at 160 °C, and keeping the autoclave in oven for another 30 min under the same reaction conditions without solid catalysts. There was no further obvious reaction occurred (**Fig. 8a**), verifying that no active sites were leached into the solution and Mn-NCA-700 was heterogeneous.

The reusability test of Mn-NCA-700 for CTH of FF was investigated at 160 °C. The monolithic catalyst could be easily separated from the solution with the assistance of tweezers after the reaction. As shown in **Fig. 8b**, there was a slight decrease in FF conversion observed in the subsequent four runs and the FA selectivity remained unchanged in all cycles. The manganese content in reaction mixture of the first and fifth reaction was extremely low (both <0.02 ppm) detected by ICP-OES analysis, suggesting that leaching of active species from Mn-NCA-700 was negligible. In addition, the monolithic architecture was stable and remained largely unchanged after the reaction (**Fig. S8a**). The recovered Mn-NCA-700 catalyst in the fifth cycle was further characterized by XRD, N₂ adsorption-desorption and TG analyses. Compared with the fresh catalyst, the crystallographic structure and porosity of spent Mn-NCA-700 all exhibited no clear changes (**Fig. S8b, c**). In contrast, the specific surface area of the used catalyst declined 16 % (to 570.2 m²·g⁻¹) and a slight weight loss in TG analysis (**Fig. S8d**) could be observed. This suggested that a small amount of organic compounds were adsorbed on the channel of carbon aerogel during reaction, which may partially block the access of active sites, thus resulting in the slightly decrease of catalytic activity.

The substrate scope for Mn-NCA-700 catalyst

Accordingly, the feasibility of the Mn-NCA-700 for CTH with a series of substrates was also investigated and the results were summarized in **Table 2**. Cellulose-derived furanic aldehydes such as 5-hydroxymethylfurfural (5-HMF) and 5-methylfurfural (5-MF), are also recognized as important platform chemicals, therefore, relevant substrate for CTH.⁵³ Clearly, the developed Mn-NCA-700 exhibited also superior catalytic performance for 5-HMF and 5-MF resulting in both more than 90% conversion with selectivities to the corresponding alcohols were 83% and 64%, respectively (**Table 2**, Entries 3 and 4). It was worth mentioning that other by-product of these two reactions was mainly 2,5-dimethylfuran,

which is a very important biofuel.⁵⁴ Furthermore, the Mn-NCA-700 was also broadly applicable for CTH of other bioderived **Table 2** CTH of different biomass-derived carbonyl compounds to alcohols.^a

Entry	Reactant	Product	Time (h)	Conv. (%)	Sel. (%)	Yield ^b (%)
1			1	99	85	84 (75)
2 ^c			0.5	99	89	88 (78)
3			1.5	91	83 ^d	76
4			2	90	64 ^d	58
5			3	100	87	87
6			6	99	81	80
7			3	94	96	90
8			4	100	92	92
9			0.7	90	90	81
10			0.8	100	97	97 (87)
11			2	99	96	95
12			4	91	99	90 (83)
13			5	100	99	99 (91)
14			2	98	99	97 (88)
15			2	100	85	85
16			10	100	91	91

^a Reaction conditions: 0.5mmol substrates in 5ml 2-propanol, 160 °C, 55mg catalyst.

^b isolated yields are given in parentheses.

^c The reaction temperature was 200 °C.

^d The main by-product is 2,5-dimethylfuran.

aldehydes. As examples, the conversions of cinnamaldehyde and citral were 99% with selectivities to the corresponding alcohols of more than 80% (Table 2, Entries 5 and 6). These corresponding alcohols are important chemical intermediates for manufacture of pharmaceuticals, flavors and cosmetics in industry. Besides the reduction of biomass-derived chemicals, other commercial aldehydes and ketones were also tested to evaluate its catalytic potential. In these reactions, all substrates were converted to corresponding alcohols with excellent conversion (90–100%) and selectivity (85–99%). However, relatively longer reaction time were needed for ketones in order to obtain satisfactory yields due to electron-donating nature of the alkyl group in ketone, for example, 1-phenylethanol was obtained from acetophenone within 10 h. This clearly suggests the Mn-NCA-700 catalyst to be a highly versatile catalyst for CTH of both biomass-derived aldehydes and other carbonyl compounds to alcohols in general.

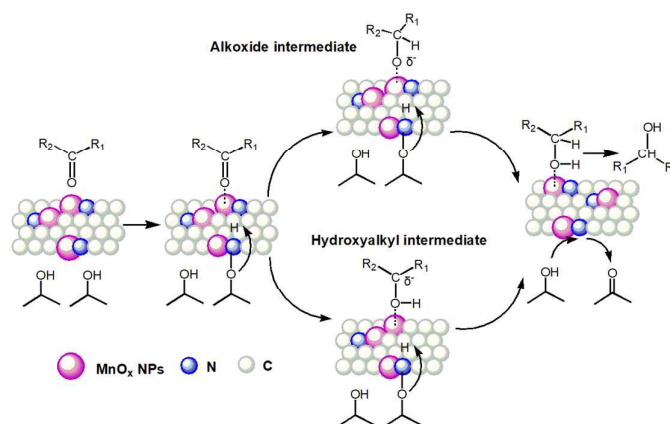
Mechanism study

So far, the transfer hydrogenation of bioderived aldehydes with 2-propanol were generally catalyzed by metal oxide catalysts without N doping. However, we demonstrated that the doped nitrogen in carbon aerogel played a crucial role in the catalytic activity of the catalyst (Table 2, Entry 3, 4, 5, 7). We speculated that the doped nitrogen in the Mn-NCA catalyst should act as basic sites (confirmed by CO₂-TPD, Fig. 6), which could promote the generation and transfer of proton to control the conversion of the reaction. According to catalysts characterization, our experimental results and the above analysis, we proposed a plausible reaction mechanism with respect to the transfer hydrogenation of carbonyl compounds to corresponding alcohols over Mn-NCA catalyst (Scheme 2). Firstly, the carbonyl compounds and 2-propanol were adsorbed on the catalysts and the N-derived basic sites in Mn-NCA captured the protons from 2-propanol to generate NH⁺ and isopropoxide by dissociation.⁵⁵ Meanwhile, the carbonyl groups in the substrate molecules was activated by electrophilic MnO_x NPs via the electron lone pair of oxygen to generate η¹(O)-aldehyde species.⁵⁶ Third, the C=O double bond was attacked by active H atom to form two active intermediates (alkoxide intermediate or hydroxyalkyl intermediate).⁵⁶ These two compounds adsorbed on MnO_x NPs surface then were hydrogenated into corresponding alcohol via the active hydrogen attack in this step. Meanwhile, 2-propanol was converted into acetone after losing two H atoms. Finally, the generated carbonyl compound and acetone was desorbed from the surface of Mn-NCA with the aiding of 2-propanol.

Conclusions

In summary, we have designed and prepared a highly efficient, monolithic and easily separated Mn-NCA catalyst by dissolving cellulose and thermolysis of cellulose-derived aerogels with uniform MnO(OH)₂ doping. A series of experiments and characterizations revealed that the monolithic hierarchically porous architecture of carbon aerogel and the synergistic

effects between homogeneously *in-situ* dispersed MnO_x NPs and surface basic sites contributed to the superior catalytic activity for transfer hydrogenation of biomass-derived



Scheme 2 Possible mechanism for the Mn-NCA-catalyzed transfer hydrogenation of carbonyl compounds.

aldehydes/ketones. Particularly, the CTH of FF on Mn-NCA-700 followed first order kinetics and resulted in activation energy of 83 kJ/mol. A plausible mechanism was also proposed. Compared with the traditional catalytic system using powdery catalyst, the developed monolithic carbon aerogel catalytic system held multiple advantages such as superior dispersibility in reactants, energy-efficient reaction process in an oven without agitation, more convenient and timesaving separation process of catalysts. Hence, this new approach for developing highly efficient monolithic catalysts from sustainable cellulose is expected to be more operational in practical application for catalytic transformation of biomass.

Experimental

Reagents

Cellulose (DP 500) as a model of biomass were supplied by Hubei Chemical Fiber Group Ltd. (Xiangfan, China). Mn(CH₃COO)₂·4H₂O (>99.0%), NaOH (>99.5%), urea (>99.5%) were purchased from Shanghai Macklin Biochemical Co., Ltd, China. Furfural (FF, >99.5%), 5-hydroxymethylfurfural (HMF, >99.0%), 5-methylfurfural (>99%), citral (>97%), cinnamaldehyde (>99.5%), veratraldehyde (>99%), 2-propanol (>99.0%) were purchased from Aladdin Industrial Corporation. All chemical reagents were obtained from commercial suppliers and used without further purification.

Preparation of different catalysts

Synthesis of Mn-NCA. The MnO_x NPs supported N-doped carbon aerogel catalysts (Mn-NCA) were prepared according to the following steps. In a typical procedure, 7 g NaOH and 12 g urea were dissolved in 81 g distilled water and the mixture solution was pre-cooled to -12.0 °C. 4 g cellulose powder was added into the above solution under mechanical agitation to

obtain a transparent cellulose solution. Subsequently, $\text{Mn}(\text{CH}_3\text{COO})_2 \cdot 4\text{H}_2\text{O}$ (7.3 mmol, 1.8 g) in aqueous solution (15% wt.%) was added to the above cellulose solution drop by drop under mechanical agitation for 5 min. The $\text{MnO}(\text{OH})_2$ doped cellulose gel (Mn-CG) was then heated for further gelation at 50 °C for 12 h. Afterwards, the obtained hydrogel was freeze-dried at -65 °C for 48 h, followed by carbonization in a horizontal tube furnace at different temperatures (600, 700, 800 °C) for 2 h under Ar flow at a heating rate of 5 °C/min. The obtained samples were immersed in 1000 mL water for 6 h and then totally washed with deionized water to remove residual chemicals. After drying at 50 °C for 12 h, samples were obtained and are denoted as Mn-NCA-T, where T stands for the carbonization temperature. Replacing $\text{Mn}(\text{CH}_3\text{COO})_2 \cdot 4\text{H}_2\text{O}$ with equimolar amounts of $(\text{CH}_3\text{COO})_2 \cdot 4\text{H}_2\text{O}$, $\text{Ni}(\text{CH}_3\text{COO})_2 \cdot 4\text{H}_2\text{O}$, $\text{Fe}(\text{CH}_3\text{COO})_2 \cdot 4\text{H}_2\text{O}$ or $\text{Cu}(\text{CH}_3\text{COO})_2 \cdot \text{H}_2\text{O}$ synthesized Co-NCA-T, Ni-NCA-T, Fe-NCA-T or Cu-NCA-T, respectively.

Synthesis of NCA-700. The procedure for preparing N-doped carbon aerogel (NCA-700) was same as that of Mn-NCA-700, but no $\text{Mn}(\text{CH}_3\text{COO})_2 \cdot 4\text{H}_2\text{O}$ saturated solution was added in the cellulose solution.

Synthesis of CA-700. The carbon aerogel without N-doping (CA-700) was prepared according to the following steps. 52 g transparent cellulose solution was directly heated at 50 °C for 12 h to obtain cellulose gels. Afterwards, the obtained hydrogel was totally washed with water to remove NaOH and urea and then impregnated with 3.5 g NaOH. The following preparation steps are the same as that of Mn-NCA-700.

Synthesis of Mn-CA-700. The MnO_x NPs supported carbon aerogel catalysts without N-doping (Mn-CA-700) was prepared according to the following steps. 58 g Mn-CG was then heated at 50 °C for 12 h for further gelation. Afterwards, the obtained hydrogel was totally washed with water to remove NaOH and urea and then impregnated with 3.5 g NaOH. The following preparation steps are the same as that of Mn-NCA-700.

Catalyst characterization

Low temperature N_2 adsorption-desorption isotherms of the materials were assessed using a Micromeritics ASAP 2020. Before measurements, the samples were outgassed at 130 °C for 8 h. The specific surface areas were evaluated using the Brunauer-Emmett-Teller (BET) method. The average pore volume and pore size were obtained by Barrett-Joyner-Halenda (BJH) method from the desorption branch of the isotherms. X-ray diffraction (XRD) patterns were recorded on a Rigaku diffractometer (D/MAX/III A, 3 kW) using $\text{Cu K}\alpha$ radiation ($\lambda = 0.1543$ nm, 40 kV, 30 mA). Organic elemental content was detected by an elemental analyzer (VarioEL III, Elementar). The manganese content of the catalysts was determined with Spectro Arcos FHX22 inductively coupled plasma-optical emission spectrometer (ICP-OES). The structures and morphologies of the materials was observed by a high-resolution scanning electron microscopy (SEM, MERLIN of ZEISS) and a high-resolution

transmission electron microscope (JEM-2100F) with EDX analysis (Bruker Xflash 5030T) operated at 200 kV. Raman spectra were completed on a LabRAM Aramis Raman Spectrometer (HORIBA Jobin Yvon) operating with 532 nm excitation and the wave number range used in the measurement was from 400 to 2000 cm^{-1} . Fourier transform infrared spectroscopy (FTIR) spectra of all samples in KBr pellet were conducted on a Bruker Vector33 spectrometer. X-ray photoelectron spectroscopy (XPS) measurements were performed on a Kratos Axis Ultra DLD system with a base pressure of 10⁻⁹ Torr. The surface basicity of catalysts was carried out via temperature-programmed desorption of CO_2 (CO_2 -TPD) by a Micromeritics AutoChem II 2920 instrument. Sample was pretreated under a flow of He (30 mL \cdot min⁻¹) at 150 °C for 2 h. Subsequently, the sample was cooled to 50 °C under He. After adsorption of CO_2 , the sample was flushed off under a helium atmosphere at 50 °C. Finally, the TPD data were collected from 50 °C–800 °C under helium (heating rate of 20 °C \cdot min⁻¹). Thermogravimetric (TG) analysis was performed using a Mettler Toledo thermal analyzer under an Ar flow (30 mL \cdot min⁻¹) from 25–700 °C (heating rate of 15 °C \cdot min⁻¹).

Procedures for the CTH of aldehydes

The CTH of aldehyde was carried out in a 10 mL stainless-steel autoclave. Typically, aldehyde (0.5 mmol), 2-propanol (5 mL), and catalyst (55 mg) were loaded into the autoclave, which was then purged with Ar and sealed. Then the reactor was put into an oven which has been heated to the desired temperature without stir. Time zero was recorded when the inside temperature of autoclave reached the target temperature. After the reaction, the reactor was rapidly placed in cold water. The monolithic catalyst was separated by a tweezers and the liquid mixtures were collected for analysis. Identification of products in the reaction mixture was conducted using GC-MS (Agilent 7890B-5977A) equipped with HP-5MS capillary column (30.0 m \times 250 mm \times 0.25 mm). The reactants and products were quantitatively analyzed on the basis of standard sample using toluene as internal standard on a GC (Shimadzu Nexis GC-2030) equipped with flame ionization detector and HP-5 capillary column (30.0 m \times 250 mm \times 0.25 mm). Product isolation was performed via column chromatography using silica gel as stationary phase and an n-pentane/ethyl acetate mixture (4:1) as eluent.

Catalyst recycling experiments

After reaction, the monolithic catalyst was separated from the solution with the assistance of tweezers, washed several times with 2-propanol and kept for the next run directly under the same reaction conditions without further treatment.

Conflicts of interest

There are no conflicts to declare.

Acknowledgments

The authors are grateful for the financial support for this work by the National Natural Science Foundation of China (21774036), Thousand Youth Talents Plan, State Key Laboratory of Pulp and Paper Engineering (No. 2017TS01) and Guangdong Province Science Foundation for Cultivating National Engineering Research Center for Efficient Utilization of Plant Fibers (2017B090903003).

Notes and references

- E. L. Kunkes, D. A. Simonetti, R. M. West, J. C. Serrano-Ruiz, C. A. Gärtner and J. A. Dumesic, *Science*, 2008, **322**, 417-421.
- D. M. Alonso, S. G. Wettstein and J. A. Dumesic, *Chem. Soc. Rev.*, 2012, **41**, 8075.
- Y. Román-Leshkov, C. J. Barrett, Z. Y. Liu and J. A. Dumesic, *Nature*, 2007, **447**, 982-985.
- H.G. Bernal, L. Bernazzani and A. M. R. Galletti, *Green Chem.*, 2014, **16**, 3734-3740.
- J. N. Chheda, Y. Román-Leshkov and J. A. Dumesic, *Green Chem.*, 2007, **9**, 342-350.
- X. Li and Y. Zhang, *Green Chem.*, 2016, **18**, 643-647.
- L. Wang and Y. X. Chen, *Green Chem.*, 2015, **17**, 5149-5153.
- G. H. Wang, X. Deng, D. Gu, K. Chen, H. Tüysüz, B. Spliethoff, H.J. Bongard, C. Weidenthaler, W. Schmidt and F. Schüth, *Angew. Chem., Int. Ed.*, 2016, **128**, 11101-11105.
- C. M. Cai, N. Nagane, R. Kumar and C. E. Wyman, *Green Chem.*, 2014, **16**, 3819-3829.
- X.L. Li, J. Deng, J. Shi, T. Pan, C. G. Yu, H. J. Xu and Y. Fu, *Green Chem.*, 2015, **17**, 1038-1046.
- M. J. Taylor, L. J. Durndell, M. A. Isaacs, C. M. A. Parlett, K. Wilson, A. F. Lee and G. Kyriakou, *Appl. Catal., B: Environ.*, 2016, **180**, 580-585.
- J. P. Lange, E. Van Der Heide, J. Van Buijtenen, R. Price, *ChemSusChem*, 2012, **5**, 150-166.
- J. He, S. Yang and A. Riisager, *Catal. Sci. Technol.*, 2017, **8**, 790-797.
- M.J. Gilkey and B. Xu, *ACS Catal.*, 2016, **6**, 1420-1436.
- J. Zhang and J. Chen, *ACS Sustainable Chem. Eng.* 2017, **5**, 5982-5993.
- F. Li, L. J. France, Z. Cai, Y. Li, S. Liu, H. Lou, J. Long and X. Li, *Appl. Catal., B: Environ.*, 2017, **214**, 67-77.
- S. Elangovan, C. Topf, S. Fischer, H. Jiao, A. Spannenberg, W. Baumann, R. Ludwig, K. Junge, M. Beller, *J. Am. Chem. Soc.*, 2016, **138**, 8809-8814.
- M. Perez, S. Elangovan, A. Spannenberg, K. Junge, Matthias Beller, *ChemSusChem*, 2017, **10**, 83-86.
- F. Wang and Z. Zhang, *ACS Sustainable Chem. Eng.*, 2016, **5**, 942-947.
- J. He, S. Yang and A. Riisager, *Catal. Sci. Technol.*, 2017, **8**, 790-797.
- W. Gong, C. Chen, Y. Zhang, H. Zhou, H. Wang, H. Zhang, Y. Zhang, G. Wang and H. Zhao, *ACS Sustainable Chem. Eng.*, 2017, **5**, 2172-2180.
- Q. Hu, L. Yang, G. Fan, F. Li, *J. Catal.*, 2016, **340**, 184-195.
- S. K. Min, S. Lim, J. Jae, J. M. Ha and H. Lee, *J. Ind. Eng. Chem.*, 2017, **52**, 59-65.
- Y. Sha, Z. Xiao, H. Zhou, K. Yang, Y. Song, N. Li, R. He, K. Zhi and Q. Liu, *Green Chem.*, 2017, **19**, 4829-4837.
- S. Rojas-Buzo, P. García-García, A. Corma, *ChemSusChem*, 2018, **11**, 432-438.
- D. Scholz, C. Aellig and I. Hermans, *ChemSusChem*, 2014, **7**, 268-275.
- M. J. Gilkey, P. Panagiotopoulou, A. V. Mironenko, G. R. Jenness, D. G. Vlachos and B. Xu, *ACS Catal.*, 2015, **5**, 3988-3994.
- B., Liu and Z. Zhang, *ACS Catal.*, 2016, **6**, 326-338.
- G. A. Somorjai, H. Frei and J. Y Park, *J. Am. Chem. Soc.* 2009, **131**, 16589-16605.
- D. M. Lai, L. Deng, Q. X. Guo and Y. Fu, *Energy Environ. Sci.*, 2011, **4**, 3552-3557.
- Z. Z. Yang, J. Deng, T. Pan, Q. X. Guo and Y. Fu, *Green Chem.*, 2012, **14**, 2986-2989.
- H. Qi, B. Schulz, T. Vad, J. Liu, E. Mäder, G. Seide and T. Gries, *ACS Appl. Mater. Interfaces*, 2015, **7**, 22404-22412.
- T. Mehling, I. Smirnova, U. Guenther and R. H. H. Neubert, *J. Non-Cryst. Solids*, 2009, **355**, 2472-2479.
- Z. Wang, T. Yokoyama, H. Chang and Y. Matsumoto, *J. Agric. Food Chem.*, 2009, **57**, 6167-6170.
- J. Yang, X. Lu, X. Liu, J. Xu, Q. Zhou and S. Zhang, *Green Chem.*, 2017, **19**, 2234-2243.
- T. Rosenau, A. Potthast, I. Adorjan, A. Hofinger, H. Sixta, H. Firgo and P. Kosma, *Cellulose*, 2002, **9**, 283-291.
- J. Cai, L. Zhang, J. Zhou, H. Qi, H. Chen, T. Kondo, X. Chen and B. Chu, *Adv. Mater.*, 2007, **19**, 821-825.
- H. Qi, Q. Yang, L. Zhang, T. Liebert and T. Heinze, *Cellulose*, 2011, **18**, 237-245.
- H. Qi, J. Liu, S. Gao and E. Mäder, *J. Mater. Chem. A*, 2013, **1**, 2161-2168.
- M. Thommes, K. Kaneko, A. V. Neimark, J. P. Olivier, F. Rodriguez-Reinoso, J. Rouquerol and K. S. W. Sing, *Pure Appl. Chem.*, 2015, **87**, 1051-1069.
- J. Shi, Y. Wang, W. Du and Z. Hou, *Carbon*, 2016, **99**, 330-337.
- B. Zhang, J. Song, G. Yang and B. Han, *Chem. Sci.*, 2014, **5**, 4656-4660.
- Y. Chu, L. Guo, B. Xi, Z. Feng, F. Wu, Y. Lin, J. Liu, D. Sun, J. Feng and Y. Qian, *Adv. Mater.*, 2018, **30**, 1704244.
- M. Liu, Z. Xiao, J. Dai, W. Zhong, Q. Xu, L. Mao, D. Yin, *Chem. Eng. J.*, 2017, **313**, 1382-1395.
- Z. Song, F. Lian, Z. Yu, L. Zhu, B. Xing and W. Qiu, *Chem. Eng. J.*, 2014, **242**, 36-42.
- X. Wang, B. Yuan, X. Zhou, Q. Xia, Y. Li, D. An and Z. Li, *Chem. Eng. J.*, 2017, **327**, 51-59.
- G. Jin, X. Xiao, S. Li, K. Zhao, Y. Wu, D. Sun and F. Wang, *Electrochim. Acta*, 2015, **178**, 689-698.
- S. Chen, D. Cai, X. Yang, Q. Chen, H. Zhan, B. Qu and T. Wang, *Electrochim. Acta*, 2017, **256**, 63-72.
- P. Hao, Z. Zhao, Y. Leng, J. Tian, Y. Sang, R.I. Boughton, C.P. Wong, H. Liu and B. Yang, *Nano Energy*, 2015, **15**, 9-23.
- J. Luo, H. Yu, H. Wang, H. Wang and F. Peng, *Chem. Eng. J.*, 2014, **240**, 434-442.
- A. Primo, P. Atienzar, E. Sanchez, J.M. Delgado and H. García, *Chem. Commun.*, 2012, **48**, 9254-9256.

Journal Name

ARTICLE

52 B. Lu, J. Liu, R. Hu, H. Wang, J. Liu and M. Zhu, *J. Mater. Chem. A*, 2017, **5**, 8555-8565.

53 R.J. van Putten, J.C. van der Waal, E. Jong, C.B. Rasrendra, H.J. Heeres and J.G. de Vries, *Chem. Rev.*, 2013, **113**, 1499-1597.

54 B. Chen, F. Li, Z. Huang and G. Yuan, *Appl. Catal., B: Environ.*, 2017, **200**, 192-199.

55 J. Long, K. Shen, Y. Li, *ACS Catal.*, 2017, **7**, 275-284.

56 S. Sitthisa, T. Sooknoi, Y. Ma, P.B. Balbuena and D.E. Resasco, *J. Catal.*, 2011, **277**, 1-13.

Table of contents



Cellulose-derived monolithic hierarchically porous MnO_x/N -doped carbon aerogel exhibited excellent catalytic activity for upgrading of lignocellulose-derived aldehydes